Tides and the Climate: Some Speculations

WALTER MUNK

Scripps Institution of Oceanography, La Jolla, California

BRUCE BILLS

Scripps Institution of Oceanography, La Jolla, California, and NASA Goddard Space Flight Center, Greenbelt, Maryland

(Manuscript received 18 May 2005, in final form 12 January 2006)

ABSTRACT

The important role of tides in the mixing of the pelagic oceans has been established by recent experiments and analyses. The tide potential is modulated by long-period orbital modulations. Previously, Loder and Garrett found evidence for the 18.6-yr lunar nodal cycle in the sea surface temperatures of shallow seas. In this paper, the possible role of the 41 000-yr variation of the obliquity of the ecliptic is considered. The obliquity modulation of tidal mixing by a few percent and the associated modulation in the meridional overturning circulation (MOC) may play a role comparable to the obliquity modulation of the incoming solar radiation (insolation), a cornerstone of the Milanković theory of ice ages. This speculation involves even more than the usual number of uncertainties found in climate speculations.

1. Introduction

An early association of tides and climate was based on energetics. Cold, dense water formed in the North Atlantic would fill up the global oceans in a few thousand years were it not for downward mixing from the warm surface layers. Mixing a stratified fluid takes energy; the required rate of energy expenditure was estimated at 2 TW (Munk and Wunsch 1998). Global tidal dissipation is 3.5 TW, two-thirds in marginal seas, one-third in the pelagic[1] oceans, suggesting a tidal contribution to the pelagic ocean mixing. Observational support comes from tidally induced fortnightly and monthly temperature variations in the Indonesian Seas (Ffield and Gordon 1996) and from measurements of ocean microstructure in the deep Brazil Basin revealing mixing over topography with enhanced intensity at spring over neap tides (Polzin et al. 1995, 1997; Ledwell et al. 2000). The Hawaii Ocean-Mixing Experiment (HOME), a major experiment along the Hawaiian Island chain dedicated to tidal mixing, confirmed an enhanced mixing at spring tides and quantified the scattering of tidal energy from barotropic into baroclinic modes over suitable topography. A few specific sites account for most of the 20 GW of barotropic tidal energy dissipation along the Hawaiian Island chain, about 2% of the 1 TW of global pelagic tidal dissipation (Egbert and Ray 2001; Merrifield et al. 2001).

The proposals for pelagic tidal mixing go back to the 1960s and 1970s (Cox and Sandstrom 1962; Bell 1975; Garrett 1979) but then fell out of fashion. The proposal for a long-period *modulation* goes back to Loder and Garrett (1978) who attributed an 18.6-yr cycle in ocean surface temperature to shallow mixing associated with the lunar nodal tide cycle. Otto Pettersson in 1910 discovered internal tides breaking over the bank that separates Gullmarfjord from the sea and spent much of his subsequent career trying in vain to convince his colleagues that tidal mixing is a factor in ocean climate (e.g., Pettersson 1930).

A few decades ago the suggestion that the Moon played a role in determining global ocean properties was considered lunatic; now it is considered obvious (Wunsch and Munk were more comfortable working in the earlier times). There is wide agreement that pelagic

[1] "relating to . . . open oceans or seas rather than waters adjacent to land or inland waters." *The American Heritage Dictionary of the English Language,* 4th ed. 2004, Houghton Mifflin.

Corresponding author address: Dr. Walter Munk, Scripps Institution of Oceanography, 9500 Gilman Dr., Mail Code 0225, La Jolla, CA 92093-0225.
E-mail: wmunk@ucsd.edu

DOI: 10.1175/JPO3002.1

TABLE 1. Equilibrium coefficients. Amplitudes are given as percent of the lunar equilibrium amplitude $K = 35.79$ cm (Doodson 1921; Cartwright and Taylor 1971; Godin 1972). Sir George Darwin (son of Charles) introduced the designations of *constituents* within the long-period, diurnal, and semidiurnal *species*; M_n is a new notation.

Doodson Nos.					
cpd	cpm	cpy	cpn	Amplitude (%)	Darwin designations
Long period ($m = 0$)					
Subannual					
0	0	0	0	73.6	Mean figure of Earth
0	0	0	1	6.6	M_n
Annual					
0	0	1	0	1.2	S_a
0	0	2	0	7.3	S_{sa}
Monthly					
0	1	0	−1	8.3	M_m
0	2	0	0	15.6	M_f
Diurnals ($m = 1$)					
1	−1	0	−1	7.1	(Nodal splitting)
1	−1	0	0	37.7	O_1
1	1	−2	0	17.6	P_1
1	1	0	0	53.1	K_1 (luni solar)
1	1	0	+1	7.2	(Nodal splitting)
Semidiurnals ($m = 2$)					
2	−1	0	0	17.4	N_2
2	0	0	−1	3.4	(Nodal splitting)
2	0	0	0	90.8	M_2
2	2	−2	0	42.4	S_2
2	2	0	0	11.5	K_2

tidal mixing must be taken into account in any realistic modeling of ocean properties. But we are a long way from understanding the underlying physics, and depend heavily on a parameterization of the processes involved.

The demonstration that tides play a role in the present ocean climate has encouraged us, prematurely perhaps, to consider a possible role of tides in past climate changes. The discussion is centered on the 41 000-yr modulation of the inclination of Earth's equatorial plane relative to the ecliptic; the modulation is caused by the gravitational pull from the other planets in the solar system. Comparable effects from precession and eccentricity are ignored for the sake of simplicity.

2. Darwin factors

Table 1 shows the amplitude of 16 selected tidal constituents [out of 400 listed by Doodson (1921)], expressed as a percentage of the lunar equilibrium amplitude

$$K = a_E \frac{m_M/m_E}{(\overline{r_M}/a_E)^3} = 35.79 \text{ cm}. \tag{1}$$

Here, a_E is the radius and m_E the mass of Earth, and m_M, $\overline{r_M}$ are the mass and mean distance of the Moon. (In many ports the tide exceeds equilibrium values, and the reader might think of the tabulated percentages as indicating centimeters of tidal *range*.)

Frequency is expressed in terms of abbreviated Doodson numbers, giving cycles per (lunar) day, month, year, and nodal period, to be designated cpd, cpm, cpy, and cpn. [The Doodson columns for lunar apsidal (8.85 yr) and solar perigee (20 900 yr) are omitted.]

The dominant constituent M_2 is at exactly 2 cpd. There is monthly splitting, with N_2, K_2 at −1, +2 cpm relative to M_2, a yearly fine structure such as S_2 at 2 cycle per *solar* day, +2 cpy, and a nodal hyperfine structure at $2 - 0.000\,15$ cpd. The spectral fine structure is the equivalent in the frequency domain to the long-term modulations in the time domain. Doodson's heroic expansion was the last gasp in the Kelvin–Darwin–Doodson development of tide prediction by adding sinusoids. Ultimately, one is better off in the time domain (Munk and Cartwright 1966; Wunsch 2000; Wunsch 2002).

The nodal modulation is too large to be ignored, yet the available tide records are usually too short to resolve the hyperfine splitting. Darwin (1911) proposed that any recorded spectral line $A\cos\omega t$ be interpreted as a temporary manifestation of a modulated signal of amplitude

$$\eta = \alpha(t)A\cos[\omega t + s(t)], \tag{2}$$

where $\alpha(t)$ is a slowly varying amplitude factor and $s(t)$ is a phase increment, both derived from equilibrium theory. "Darwin factors" are related according to

$$\alpha\cos s = 1 + \varepsilon\cos N \quad \text{and} \quad \alpha\sin s = +\varepsilon\sin N,$$

or, to first order in ε,

$$\alpha = 1 + \varepsilon\cos N \quad \text{and} \quad s = +\varepsilon\sin N, \tag{3}$$

with N increasing by 2π rad in 18.61 yr at a rate $\dot{N} = dN/dt$. Substituting in (2) yields

$$\eta = A\cos\omega t + \varepsilon A\cos(\omega + \dot{N})t. \tag{4}$$

The spectrum consists of a line at the principal frequency ω, plus a single weak sideband at a slightly lower frequency $\omega + \dot{N}$ ($\dot{N}$ is negative for the nodal regression). For M_2, the fractional amplitude of the split line is $\varepsilon = 3.4/90.8 = 0.037$.

The nodal tide M_n (as well as other long-period tides) appear in two places in Table 1: (i) at the primary frequencies and their harmonics, for example, M_m, $M_f = 1$, 2 cpm; S_a, $S_{\text{sa}} = 1, 2$ cpy; $M_n = 1$ cpn; and (ii) in *splitting* the principal short-period constituents. The mixing problem involves the split high-frequency constituents

(ii), and *not* the primary lines (i) for the following reason: mixing is associated with the tidal current u, and *not* the tidal elevation η. Long-period tidal currents are very weak. For a basin of length L and depth H, the horizontal particle[2] velocity scales as

$$u = \frac{L}{HT}\eta, \tag{5}$$

where T is the characteristic period. For $L = 1000$ km, $H = 1$ km, and $T = 18.6$ yr, we have $u = 10^{-6}$ m s^{-1}.

3. Loder and Garrett on nodal mixing

Loder and Garrett (1978, hereinafter LG) base their analysis on the published values (Godin 1972) of the split constituents with fractional amplitude modulations

$$\frac{7.2}{53.4} = 11\%(K_1), \quad \frac{7.1}{37.7} = 19\%(O_1), \quad \text{and} \quad \frac{3.4}{90.8} = 3.7\%(M_2). \tag{6}$$

The diurnals K_1, O_1 have roughly half the amplitude of the principal semidiurnal constituent M_2 but a much larger *fractional* modulation. There is an important consideration with regard to the phase of the modulation. Whereas the semidiurnals are strongest when the Moon is closest to the equatorial plane (at 18.6-yr intervals), the diurnals are then weakest. We emphasize that although the modulation is of very low frequency, we are here concerned with the relatively high frequency semidiurnal and diurnal spectral bands.

Next LG refer to certain relations for turbulent mixing in unstratified water:

$$\kappa = \frac{u^{*2}}{200f}, \quad u^{*2} = \gamma u^2, \quad \text{provided} \frac{fH}{u^*} > 0.1, \tag{7}$$

where κ is the turbulent diffusivity, f is the Coriolis parameter, H is depth, and $\gamma = 2.5 \times 10^{-3}$ is the bottom drag coefficient. Thus, κ is quadratically dependent on the tidal current u. For a modulation at frequency σ of the ω tide

$$(\eta, u) = (A, U)(1 + \varepsilon \cos\sigma t)\cos\omega t, \tag{8}$$

we have

$$\kappa = \kappa_0(1 + \varepsilon \cos\sigma t)^2 = \kappa_0(1 + 2\varepsilon \cos\sigma t + \cdot\ \cdot\ \cdot). \tag{9}$$

To interpret the nodal variation in diffusivity, LG solve the temperature diffusion equation

$$\frac{\partial\theta}{\partial t} = \kappa \frac{\partial^2\theta}{\partial z^2} \tag{10}$$

for a constant heat flow Q through the surface at $z = H$ and zero heat flow through the bottom $z = 0$. The initial temperature $\theta(z, 0) = \theta_0$, a constant. Loder and Garrett (1978) write the solution

$$\theta(z, t) = \theta_0 + \dot{\theta}_0 t + \frac{1}{2}(\dot{\theta}_0/\kappa)(z^2 - \frac{1}{3}H^2), \quad t \gg \tau, \tag{11}$$

where $\dot{\theta}_0 \equiv Q/(\rho C_p H)$ is the warming of the entire water column, and $\tau = H^2/\kappa$ is the characteristic diffusion time. The assumption $t \gg \tau$ limits the validity to turbulent coastal waters. The top-to-bottom temperature difference is then $\theta(H, t) - \theta(0, t) = \frac{1}{2}\dot{\theta}_0\tau$. A fractional increase ε in the tidal potential increases κ to $\kappa_0(1 + 2\varepsilon)$ and *decreases* the surface temperature by a fraction $\frac{4}{3}\varepsilon$ of the top-to-bottom temperature difference:

$$\delta\theta = \frac{4}{3}\varepsilon[\theta(H) - \theta(0)]. \tag{12}$$

Typically, this is on the order of a few tenths of degree. In regions with dominant semidiurnal tides, SST minima are expected around 1886, 1904, 1923, 1941, 1960, 1978, 1997, 2015, . . . (when the Moon's orbit is most nearly equatorial). In regions dominated by the diurnal species, SST maxima are to be expected at these times.

These expectations are fulfilled. Loder and Garrett (1978) examined 12 stations with records extending over 30–70 yr; six stations dominated by diurnal tidal currents and six stations by semidiurnal tidal currents. The nodal cycle contributes only 20% to the variance of annual mean SSTs, not adequate to show conclusive evidence for a spectral peak at the nodal frequency. Even so, "The coincidence of the phase of the fitted nodal cycle with the phase of the tidal variation is remarkable, and seems to be good evidence. . . ." (Loder and Garrett 1978).

4. Obliquity versus nodal modulation

In estimating a possible role for the obliquity modulations, we need to discuss similarities and differences with the nodal modulations. Unlike the LG analysis, we have no recorded data for testing the speculation. The reviewer has suggested that quantities such as the paleostratification are probably more readily interpreted as related to tidal mixing than to insolation.

The long chain of arguments is outlined below.

1) The tidal potential induces a spheroidal distortion in the figure of Earth, with elongations toward and

[2] The usual terminology "orbital" (as distinct from "phase") velocity here leads to a confusion with orbital planetary motion.

away from the tide-producing body; for a fixed position of the tide-producing body, this would appear as a zero-frequency term in the tidal expansion (Table 1). Monthly, yearly, and other long-period variations in the positions of the Moon, Earth, and the Sun shift some of the zero-frequency variance into the long-period species. The diurnal rotation of Earth generates semidiurnal and diurnal frequencies, akin to a conversion from DC to AC electric current. The semidiurnal and diurnal spectra in tide potential are complex spectral clusters, with cpm, cpy, and cpn fine structure related to the nonlinearity of Newton–Kepler (NK) orbital dynamics (tidal potential $\sim 1/r^3$).

2) The long-period ocean *forcing* is *not* attributed to the primary long-period tidal species (18.6 yr, 41 000 yr) but to the spectral fine structure in the semidiurnal and diurnal species. The reason is that mixing is associated with the particle velocity u not the elevation η, and for the long-period species u is extremely small, of order 1 μm s^{-1} [Eq. (5)]. The long-period ocean *response* is the result of the nonlinearities in Navier–Stokes (NS) fluid dynamics responding to the difference frequencies in the complex SD and D tide potential clusters.
3) So far, the discussion holds for both the nodal and obliquity variability. Loder and Garrett (1978) related the nodal tide to an 18.6-yr variability of SST in coastal waters, using a simple diffusion equation for guidance. They chose a quadratic nonlinearity, $\kappa \sim \langle u^2 \rangle$, based on boundary layer turbulence in nonstratified fluids. These processes are not applicable to tidally produced turbulence in the pelagic oceans. (But we end up using the same $\kappa \sim \langle u^2 \rangle$ proxy: it is traditional and simple, and does not offend any presently known evidence.)
4) We associate the pelagic stirring and mixing to Richardson-type instabilities provided by internal tides. The instability is associated with an increase of the (inverted) ambient Richardson number $(du/dz)^2/N^2$ to some critical value. Internal tides contribute by an increase in the numerator and a decrease in the denominator; by an enhancement in the ambient shear, and by a divergence of neighboring isopycnals. These effects of shearing and straining in the internal tide field are of comparable magnitude and are expected to lead to enhanced turbulent mixing.
5) Loder and Garrett (1978) considered a perturbation in the near-surface temperature gradient in a diffusive model. Here, we consider the variation of temperature in the entire water column, using a diffusion–advection model for guidance. Next, we estimate the variability in the poleward flux of heat as a consequence of the temperature perturbation, using a simple model of the meridional overturning circulation (MOC). These are two independent steps, each subject to great uncertainty. Pelagic turbulence involves nearly all of physical oceanography and is not well understood.
6) Nodal and obliquity variabilities in the tidal current u (as well as height η) are proportional to the variability in the tidal potential V. For the nodal modulation, V is proportional to the inclination of the Moon's orbit relative to the ecliptic by 5.1°; for the obliquity modulation, the determining factor is the variation 23.5° ± 1.0° of the obliquity itself. The squared potential $\langle V^2(t) \rangle$ of the SD species varies by 7.8% and 1.5% for nodal and obliquity modulations, respectively.
7) The fractional modulation of 7.8% by the nodal tides is associated with changes in surface temperature by only a few tenths of degrees and is difficult to detect. The fractional variation in diffusivity of 1.5% by the obliquity tide is even smaller. Yet the ratio in periods is of order 2000:1. Given the appropriate long time constants of global ocean overturning, the weak obliquity tides might play a role in ocean climate; it is a matter of joules versus watts. The magnitude of the MOC variability may be comparable to that of the incoming solar radiation (insolation). Both depend on the obliquity time scale, but the detailed time histories differ, with the tides depending on the lunar and solar orbits, but insolation depending only on the solar orbit perturbations.

5. Tide potential

We need to sketch the derivation of the nodal and obliquity perturbations. The height of the "equilibrium tide" is given by

$$\eta_{\rm eq} \equiv \frac{V}{g} = K\left(\frac{r}{\bar{r}}\right)^3 P_2(\mu), \quad K = a\,\frac{m_M}{m_E}\left(\frac{a}{\bar{r}}\right)^3 = 35.8 \text{ cm},$$

where $P_2(\mu)$ is the Legendre polynomial of degree $n = 2$ (the case of interest) and $\mu = \cos\gamma$, where $\gamma(t)$ is the angular distance between source and station coordinates: the sublunar (subsolar) latitude $\theta(t)$ and longitude $\lambda(t)$, and the fixed station coordinates θ^*, λ^*. Simple geometry relates $P_2(\mu)$ to the associated Legendre function $P_2^m(\mu)$:

$$P_2(\cos\gamma) \sim \sum_{m=0}^{2} P_2^m(\theta) e^{im\lambda} P_2^m(\theta^*) e^{im\lambda^*}.$$

Using the normalization of the Legendre functions by Munk and Cartwright (1966) and Cartwright and Taylor (1971),

$$P_2^0(\theta) = \frac{3}{2}\sin^2\theta - \frac{1}{2}, \quad P_2^1 = 3\sin\theta\cos\theta, \quad \text{and}$$

$$P_2^2 = 3\cos^2\theta, \tag{13}$$

corresponding to the long-period, diurnal, and semidiurnal species. For fixed station coordinates θ^*, λ^*, Eq. (13) relates the tidal potential to the latitude $\theta(t)$ and longitude $\lambda(t)$ of the sublunar (subsolar) point.

The diffusivity at a given station is taken to vary as $\kappa \sim (p_2^m)^2$. There are daily variations between the times of flood tide and slack tide, and monthly variations between spring and neap tides. Suppose these have been duly averaged (see later), yielding $\bar{\kappa}$, which varies slowly in the course of a year and at longer time scales.

The solar inclination relative to the equator varies from $\varepsilon = +23.5°$ in summer to $\varepsilon = -23.5°$ in winter, according to

$$\sin\theta(L) = \sin\varepsilon\sin L, \quad 0 \le L \le 2\pi,$$

where L is the mean solar longitude. The required annual mean-square values

$$f \equiv \langle (P_2^m)^2 \rangle (2\pi)^{-1} \int_0^{2\pi} (P_2^m)^2\, dL \quad \text{are}$$

$$f_{\rm LP} = \frac{1}{4} - \frac{3}{4}\sin^2\varepsilon + \frac{27}{32}\sin^4\varepsilon, \quad f_D = 9\left(\frac{1}{2} - \frac{3}{8}\sin^2\varepsilon\right)\sin^2\varepsilon,$$

and

$$f_{\rm SD} = 9\left(1 - \sin^2\varepsilon + \frac{3}{8}\sin^4\varepsilon\right) \tag{14}$$

for the long-period, diurnal, and semidiurnal species, respectively (Fig. 1). With increasing obliquity ε, the f functions *decrease* for the semidiurnal species [which are largest for the Moon (Sun) at the equator], but *increase* for the diurnal species (which vanish at zero obliquity); this accounts for the 180° phase difference between the diurnal and semidiurnal species as observed by LG.

Relative to the ecliptic pole the lunar orbit pole is inclined at a nearly constant angle of 5.1° and Earth's spin pole remains near 23.5°. The plane of the lunar orbit precesses with a period of 18.6 yr in response to the solar attraction. Lunar tides on the planet Earth depend on the angle of the lunar pole relative to Earth's spin pole and are highly variable, with extreme values $\varepsilon_M = 23.5° \pm 5.1°$. The f function varies by $\Delta f = f(28.6°) - f(18.4°)$, with a fractional variation

$$\frac{\frac{1}{2}\Delta f}{f(23.5°)} = -20\%(\text{LP}), \quad +35\%(D), \quad \text{and} \quad -6.7\%(\text{SD}), \tag{15}$$

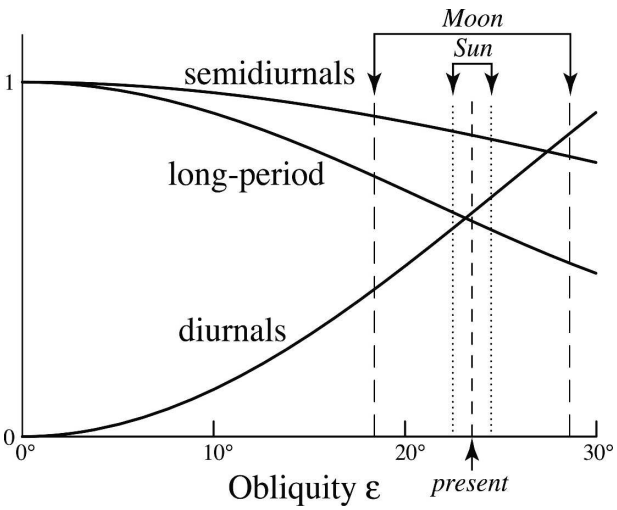

FIG. 1. Mean-square tide potential for the semidiurnal, diurnal, and long-period tide species. Semidiurnal and long-period tides are largest if the tide-producing body is in the equatorial plane (obliquity = 0). Diurnal tides vanish for zero obliquity. The curves are nomalized to correspond to $\frac{1}{9}f_{\rm SD}$, f_D, and $4f_{\rm LP}$, where $f(\varepsilon)$ are the functions in Eq. (14).

as compared with the +22% (K_1), +38% (O_1), and −7.4% (M_2) used by LG [2 times the values in Eq. (6) to allow for squaring]. Here, K_1 depends on both lunar and solar forcing and this accounts for the lower value (22%) as compared with O_1 (38%).

The obliquity modulations are easily estimated. Taking averages over the nodal period, further variations are associated with the variable inclination of the equatorial plane relative to the ecliptic due to the pull on Earth by other planets, principally Venus (because it is so close) and Jupiter (because it is so massive). The obliquity varies between 22.5° and 24.5° and is now very near the central value. The result is

$$\frac{\frac{1}{2}\Delta f}{f(23.5°)} = -4\%(\text{LP}), \quad +6.9\%(D), \quad \text{and} \quad -1.3\%(\text{SD}). \tag{16}$$

Perhaps the traditional separation into the long-period, diurnal, and semidiurnal species is not called for, and one should have a single discussion in the (variable) plane of the tide-producing forces.

6. Quadratic nonlinearities

We now consider various sources of generating long-period modulations (Fig. 2). The simplest case is that of the Sun and Moon pulling in the same and opposite directions at fortnightly intervals, thus producing the strong fortnightly modulation. The trigonometric identity

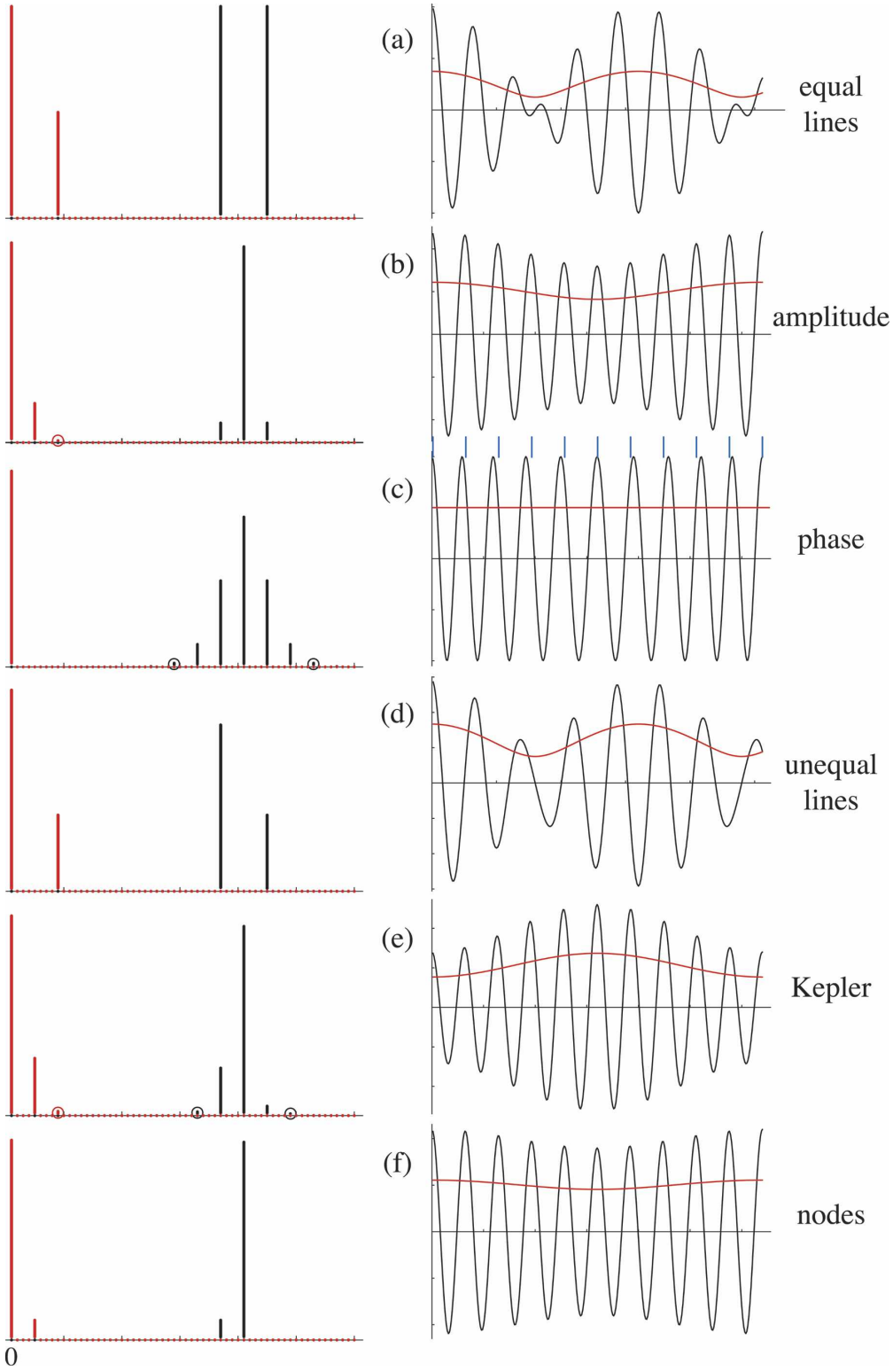

FIG. 2. Cartoons illustrating low-frequency forcing (red) resulting from nonlinear interactions between high-frequency tidal constituents (black) in the (left) frequency and (right) time domains. The tide potentials associated with (e) a Kepler elliptic orbit and (f) the regression of the lunar nodes are compared with (a)–(d) various elementary models.

$$\cos x_1 + \cos x_2 = 2\cos\frac{1}{2}(x_1 - x_2)\cos\frac{1}{2}(x_1 + x_2),$$
$$x_i = w_i t, \tag{17}$$

renders the two-body forcing indistinguishable from an excitation at the mean frequency whose amplitude is modulated at half the difference frequency. Since Newton–Kepler dynamics is linear with regard to the superposition of two tide-producing bodies (no gravitational interaction), there is no lunar excitation at the fortnightly frequency, only the interference pattern (as from two independent turning forks). Low-frequency forcing depends entirely on the Navier–Stokes nonlinearities, as portrayed by a squaring devise (case a).

For a near-circular orbit with eccentricity e there will be both amplitude and phase modulation. Consider the simple cases of amplitude modulation only (case b) and phase modulation (case c), according to $\eta = A\cos(\omega t + s)$, with

$$A(t) = 1 + \varepsilon\cos\sigma t \quad \text{and} \quad s(t) = \varepsilon\sin\sigma t,$$

where ε is a small parameter and $\sigma \ll \omega$. For the amplitude modulation, the linear high-frequency triplet at $\omega - \sigma$, ω, and $\omega + \sigma$, upon squaring, produces low frequencies 0, σ (order 1, ε) (in addition to high frequencies, which we ignore). For pure phase modulation, the original spectrum extends beyond the triplet, but the low frequencies of the squared spectrum are very weak.

Case d for two independent (but unequal) lines (in the ratio 0.458 of solar to lunar forcing) is not fundamentally different from case a. For the Kepler orbit (case e), to first order

$$r = r_0(1 + \varepsilon\cos s_0), \quad s = s_0 - 2\varepsilon\sin s_0, \quad \text{and} \quad s_0 = \sigma t \tag{18}$$

so that the "swept area"

$$r\frac{1}{2}rds = \frac{1}{2}r_0^2(1 + 2\varepsilon\cos_0)(ds_0 - 2\varepsilon\cos s_0 ds_0) \approx \frac{1}{2}r_0^2 ds_0$$

remains constant. The equilibrium tide equals

$$\eta = A(r/r_0)^{-3}\cos[\omega t + s(t)]$$
$$= A\cos\omega t - \frac{3}{2}\varepsilon A[\cos(\omega + \sigma)t + \cos(\omega - \sigma)t]$$
$$+ \varepsilon A[\sin(\omega + \sigma)t + \sin(\omega - \sigma)t]. \tag{19}$$

Amplitude and phase modulation are in the ratio 1.5:1, and in quadrature. Squaring leads to 0, σ, 2σ frequencies. The contribution of the phase modulation to the squared record is negligible.

Kepler splitting differs from *nodal* splitting. The "ascending node" (the point where the Moon crosses from south to north of the ecliptic plane) travels westward, completing an orbit in 18.61 yr. The result is the single sideband of the Darwin factors [Eq. (4)]. Obliquity is more akin to an amplitude modulation, and gives a split triplet. Monthly, yearly, nodal, and obliquity modulations are quite distinct, yet the results of squaring and averaging are similar. Similar comments apply to nonlinearities other than squaring.

7. Internal tides and shear instability

Consider first, the long surface waves ($kH \ll 1$) of small amplitude ($A/H \ll 1$), with

$$\eta = A\cos(kx - \omega t) \quad \text{and} \quad u = U\cos(kx - \omega t) \tag{20}$$

designating vertical displacement and horizontal particle velocity. Conservation of mass requires $H\,\partial u/\partial x = -\partial\eta/\partial t$, or

$$\frac{U}{C} = \frac{A}{H}, \quad C = \frac{\omega}{k} = \sqrt{gH}. \tag{21}$$

For a horizontal *displacement* $\xi = B\sin(kx - \omega t)$, we have $-B\omega = U$ and from (21)

$$\left|\frac{A}{B}\right| = kH \ll 1. \tag{22}$$

For $H = 4$ km, $T = 12.4^h$, $C = 200$ m s^{-1}, $\lambda = CT = 8920$ km, $kH = 0.0028$, and $A = 0.5$ m, we have $B = 177$ m.

For a sloping bottom, $m = 0.1$ say, the horizontal displacement B is associated with a vertical displacement

$$mB = \frac{mA}{kh} = 18\text{ m}. \tag{23}$$

Under suitable bottom conditions, surface tides will scatter into internal tides with amplitudes of order $A_{\text{IT}} = mB$ (18 m), larger that the amplitude of the surface tide (0.5 m).

Simmons et al. (2004b) parameterizes ocean mixing by a diffusivity

$$\kappa = \kappa_0 + \Gamma\varepsilon/N^2, \quad \varepsilon = \frac{1}{2}NL_B^{-1}H^2L_T^{-1}F(z)\langle u^2\rangle, \tag{24}$$

where ε is the tidal dissipation per unit mass (dimension m^2 s^{-3}). Here, Γ is the mixing efficiency, L_B and H are the length and height scales of bottom roughness, and $F(z)$ is a vertical turbulence structure function with scale L_T. Note the dependence on the squared tidal particle velocity u^2, the pelagic equivalent to Eq. (7).

All these parameters can be tuned to provide the expected magnitudes. They tell us nothing about the

physical processes involved in turning tidal energy into turbulent mixing. We can gain some insight from recent measurements on (Alford and Pinkel 2000). Topographic scattering produces multiple internal tide modes. The intensive modes 1 and 2 radiate away from the island chain and can be traced over 1000 km by satellite altimetry. There appear to be strong resonant interactions accompanied by turbulent mixing at latitude 28.9° where the Coriolis parameter f equals half the M_2 frequency. The radiating low modes may convert into the internal wave continuum and power some of the pelagic mixing.

The high modes, 3, 4, . . . , are locally dissipated. HOME has found evidence for separate instabilities associated with the shear and strain of internal tides at the flank of Kaena Ridge (Pinkel et al. 2000). The strain instabilities occur 6–9 h later than the shear instabilities.

Instabilities occur for large root-reciprocal Richardson numbers:

$$\mathrm{Ri}^{-1/2} = \frac{|du/dz|}{N}, \quad N^2 = -\frac{g}{\rho}\frac{d\rho}{\partial z},$$

where N is the buoyancy (Brunt–Väisälä) frequency. Large $\mathrm{Ri}^{-1/2}$ is associated with large shear (du/dz) and weak stratification (low $d\rho/dz$). Increased positive strain separates the distance between adjoining isopycnals and so reduces N^2 to $N^2(1 - d\eta/dz)$.

Let $\mathrm{Ri}_0^{-1/2} = (dU_0/dz)/N_0$ represent the ambient condition, with

$$u \sim \cos kx \cos kz \cos\omega t \quad \text{and} \quad \eta \sim \sin kx \sin mz \sin\omega t, \tag{25}$$

designating a system of superimposed internal waves. Then,

$$\mathrm{Ri}^{-1} = \frac{(U_0' + u')^2}{N_0^2(1 - \eta')} \approx \mathrm{Ri}_0^{-1}\left(1 + \frac{2u'}{U_0'} + \eta'\right), \tag{26}$$

where $u' = du/dz$, and so on. Then using $\partial u/\partial x = -\partial w/\partial y = -\partial^2\eta/\partial t\partial y$ and the internal wave dispersion $\omega/N = k/m$, we end up with

$$\mathrm{Ri}^{-1} = \mathrm{Ri}_0^{-1}\left(1 + \frac{2u'}{U_0'} + i\mathrm{Ri}_0^{-1/2}\frac{u'}{U_0'}\right). \tag{27}$$

For a near-critical ambient $\mathrm{Ri}_0 \approx \frac{1}{4}$, the strain and shear instabilities are of equal magnitude and in quadrature.

In summary, the conversion of pelagic tidal energy into mixing energy is a manifold process that is not understood (St. Laurent and Garrett 2002; Garrett 2003; Simmons et al. 2004a,b). We simply do not have a good rule for the conversion of tidal energy into pelagic mixing, and the assumed dependence on the squared potential is a matter of simplicity, not understanding.

8. Ocean time scales

We have considered tidal modulations on various time scales. Take a quasi diffusivity that varies as the square of the tidal potential. The spring–neap modulation is of order 1, but the duration is too short to have any climate implications. Other perturbations are of order of a few percent, but with vastly different time scales: month, year, 18.6 yr, and 41 000 yr.

For an ocean of depth $H = 4000$ m, with diffusivity $\kappa = 10^{-4}\ \mathrm{m^2\ s^{-1}}$, and upwelling velocity $w = 10^{-7}\ \mathrm{m\ s^{-1}}$ [corresponding to 25 Sv (Sv $\equiv 10^6\ \mathrm{m^3\ s^{-1}}$) of deep-water formation], we can define three time scales:

$$\kappa/w^2 = 300y, \quad H/w = 1300y, \quad \text{and} \quad H^2/\kappa = 5,000y.$$

All three scales are long relative to the nodal modulation, and accordingly the nodally modulated tidal energy $\langle V^2\rangle$ is a good measure of the *instantaneous* ocean mixing. The obliquity forcing has a period long compared to the ocean time scales. The equator-to-Pole heat flux is a time-integrated measure (over 10 000 yr, say) of obliquity mixing variability.

9. Poleward heat flux

An increase in flux lowers the equatorial temperature and raises the polar temperature. For a simple model[3] of a meridional overturning circulation (MOC), set

$$v(z) = V(1 - 2z/d)\sin[k(z)z], \quad k(z) = k_0(1 - z/d), \tag{28}$$

for the volume flux across 30°N (say). The constants

$$d = 10.5\ \mathrm{km}, \quad k_0 = 2.44\ \mathrm{km^{-1}}, \quad \text{and} \quad V = 1.22$$

are so chosen that the flow is northward above a depth $h = 1.5$ km, southward beneath h, and vanishes at the surface $z = 0$ and the bottom $z = H = 4.5$ km (Fig. 3). Here, V is a scaling factor such that the integrated volume flux (dimensionless) between 0 and h is $+1$ and between h and H is -1.

We take an exponential temperature profile

$$T(z; p) = T_0\exp(-pz), \quad p = w/\kappa = 1\ \mathrm{km^{-1}}, \tag{29}$$

[3] The model is adopted for computational convenience. The actual situation differs greatly from ocean to ocean.

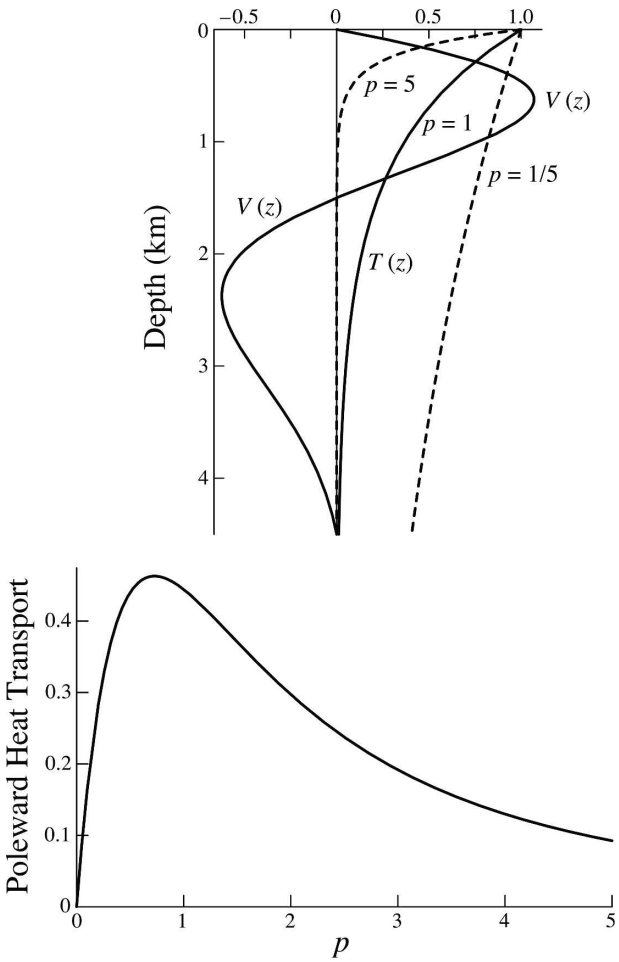

FIG. 3. Assumed current profile $V(z)$ of the meridional overturning circulation, so normalized that the integrated volume transport between the surface and the node at $h = 1.5$ km $= +1$, and between h and the bottom, is 1. The top-to-bottom heat transport for a temperature profile is $T(z) = \exp(-pz)$ and has a maximum near $p = 1$.

for a simple model of diffusive–convective balance, with $w = 10^{-7}$ m s^{-1} (consistent with $Q = 25$ Sv), $\kappa = 10^{-4}$ m^2 s^{-1}, $\rho = 1026$ kg m^{-3}, $C_p = 3994$ J kg^{-1} °C^{-1}, and $T_0 = 20$°C. A scale factor for the integrated heat flux is

$$F(p) = \int_0^H dz\, \upsilon(z) T(z; p). \tag{30}$$

Then, $F(0) \to 0$ (uniform temperature) because there is equal volume flux northward and southward; $F(\infty) \to 0$ corresponding to a infinitely thin warm surface layer where the flow vanishes. For $p = 1$, $F(1) = 0.46$, the total poleward heat flow is

$$\text{PHF} = \rho C_p T_0 Q F(1) = 0.95 \times 10^{15} \text{ W}. \tag{31}$$

Simmons et al. (2004b) have examined two models of tidally driven mixing in a numerical model of the general ocean circulation. At 30°N the two models produce 1.2 and 0.8×10^{15} W, respectively, of poleward heat transport.

For orientation, consider a perturbation $T(z)$, leaving $\upsilon(z)$ unchanged (this is highly unrealistic). The change in poleward heat transport can be positive or negative, depending on the value of p. For our choice of $p = 1$ km^{-1}, a 1% *increase* in diffusivity κ is accompanied by a 1% *decrease* in p, and a 0.3% *increase* in poleward heat flux. This differs in sign from the result of Simmons et al. (2004b), and compounds the ambiguity associated with the opposite sign in the response of the semidiurnal and diurnal tides to the obliquity modulation [Eq. 16)]. We end up with an effect of (allegedly) significant magnitude but unknown sign, hardly a satisfactory situation.

10. Insolation

We compare the perturbation in the tide-producing forces to the perturbation in the incoming solar radiation. They have quite similar spectra, both dominated by obliquity, but they differ in three important aspects: (i) radiation is entirely of solar origin, whereas both the Moon and Sun contribute to the tides; (ii) Earth is opaque to radiation and transparent to gravitation; "clipping" associated with the opacity renders the radiation spectrum more complex; and (iii) solar radiation directly delivers energy to Earth's surface, whereas tidal mixing modifies the poleward transport of heat by the MOC, with large (and unknown) phase lag.

On an annual- and diurnal-averaged basis, insolation varies with the terrestrial latitude θ^* according to

$$\iota = \frac{S}{4\sqrt{1-e^2}}\left[1 - \frac{5}{2}\left(1 - \frac{3}{2}\sin^2\varepsilon\right)P_2^0(\theta^*)\right]$$
$$\equiv \iota_0(e) + \Delta\iota(e, \varepsilon)P_2^0(\theta^*). \tag{32}$$

Eccentricity e and obliquity ε influence the pattern quite differently. Eccentricity changes the global mean, but does not influence the spatial pattern. Obliquity does not change the global mean but does influence the Pole-to-equator gradient. The first term $\iota_0(e)$ is balanced by back radiation and determines the mean temperature. The second term varies from $-\Delta\iota P_2^0(\theta^*) = +\frac{1}{2}\Delta\iota$ at the equator, to $-\Delta\iota$ at the Poles, and vanishes at $\theta_0^* = \pm\text{arc}\sin(1/\sqrt{3}) = \pm 36.25°$. The total area-weighted fluxes between the equator and θ_0^*, and between θ_0^* and the Poles are $\pm(\sqrt{3}/9)\Delta\iota$, respectively. [The reviewer has pointed out that higher-order terms in Eq. (32) (Rubincam 1994) change the hinge latitude

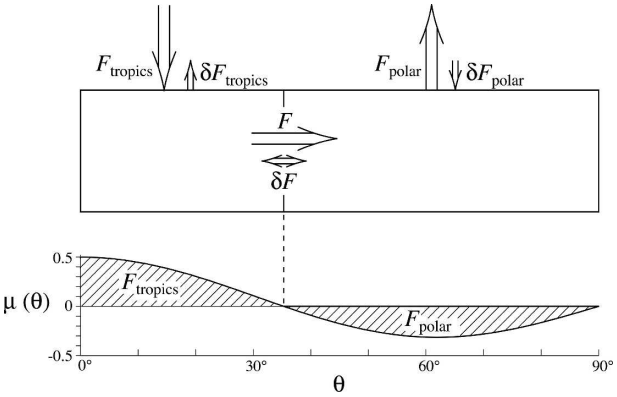

FIG. 4. (top) Sketch of proposed radiative balance. (bottom) The assumed radiative flux density relative to a mean radiation, with a zero crossing at 36° latitude; in a steady state the integrated tropical excess equals the polar deficit, and the poleward transport of heat across the zero latitude: $F_{\text{Tropics}} = F_{\text{polar}} = F$. A variable obliquity modulates the incoming radiation by $\delta F_{\text{Tropics}}$, δF_{polar} and independently modulates the poleward transport by δF.

from 36° to 43° and significantly alter the area-weighted fluxes.]

Equilibrium is maintained by a poleward flux across θ_0^* of $(\sqrt{3}/9)\Delta\iota(e, \varepsilon_0)$ W (neglecting the small difference in tropical and polar back radiation). The fractional departure from equilibrium associated with the obliquity variation from 22.5° to 24.5° is given by

$$\frac{\frac{3}{4}[\sin^2(24.5°) - \sin^2(22.5°)]}{1 - \frac{3}{2}\sin^2(23.5°)} = 2.6\%. \tag{33}$$

Increased obliquity increases the polar radiation and decreases the tropical radiation (Fig. 4). Equation (33) can be compared to the fractional perturbation in the squared semidiurnal tidal potential [Eq. (14) to order ε^2],

$$\frac{\frac{1}{2}\sin^2(24.5°) - \sin^2(22.5°)}{1 - \frac{1}{2}\sin^2(23.5°)} = 1.5\%. \tag{34}$$

Fractional perturbation in radiation and the mean-square tide potential are of the same order (not surprisingly). Increasing obliquity increases incoming polar radiation, decreases the semidiurnal $\langle V^2 \rangle$, but may increase or decrease the poleward ocean heat flux.

11. Ice ages

The role of obliquity in marine $\delta^{18}O$ records was first shown by Hays et al. (1976), but the original associations of ice ages with orbital perturbations of insolation go back to Croll (1890) and Milanković (1941). There has always been the problem of reconciling the 40-kyr obliquity period with the 100-kyr scale of ice ages. A simple remedy is to assign to the obliquity the role of a pacemaker that terminates the ice sheets every second or third obliquity cycle at times of high obliquity. Huybers and Wunsch (2005) have examined the last seven terminations (the best-defined features of the paleotemperature records) and find that "the null hypothesis that glacial terminations are independent of obliquity is rejected at the 5% significance level."

Accordingly, the terminations are timed by obliquity, whatever the manifestation: orbital perturbations in the incoming solar radiation, the traditional view, or tidal modulations in the meridional ocean heat flux. Figure 5 shows the time histories of insolation and semidiurnal tidal equilibrium *energy* plotted side by side (for better comparison the sign for the tidal energy is reversed since high obliquity results in low tidal energy). We have ignored eccentricity; it is now included and accounts for a high variability in the obliquity cycles of insolation and tidal energy. The obliquity perturbations take into account the gravitational pull from *all* of the planets in the solar system.

Fractional changes are roughly by ±2% for insolation and by ±1% for tidal energy. But here the comparison ends. Whereas insolation has a direct interpretation for climate change, the tidally related heat flux $F(t)$ is related to the tide potential $V(t)$ in a most complex way, as we have seen. We express this symbolically by the convolution integral

$$\frac{\delta F}{F} = \Phi^* \frac{\delta V^2}{V^2},$$

where Φ includes nearly all that is unknown in oceanography. In the most recent termination, global sea level started rising at −20 kyr, and had reached 100 m (out of 120 m total) by the time (−10 kyr) the insolation (obliquity) was at a maximum (Munk 2002). One would feel more comfortable if the obliquity forcing were advanced by 10 000 yr, and there are many ways to do so with the additional degrees of freedom afforded by including tidal mixing (we have withstood the temptation). There are other complexities. The rising sea level *significantly* alters the depth and dissipation in the shallow seas; Egbert et al. (2004) estimate that the North Atlantic tides during glacial times were 2 times as high and the pelagic dissipation almost three times the present rate. These feedbacks dwarf the astronomic forcing.

But the numbers will not go away. It takes 10^{25} J to

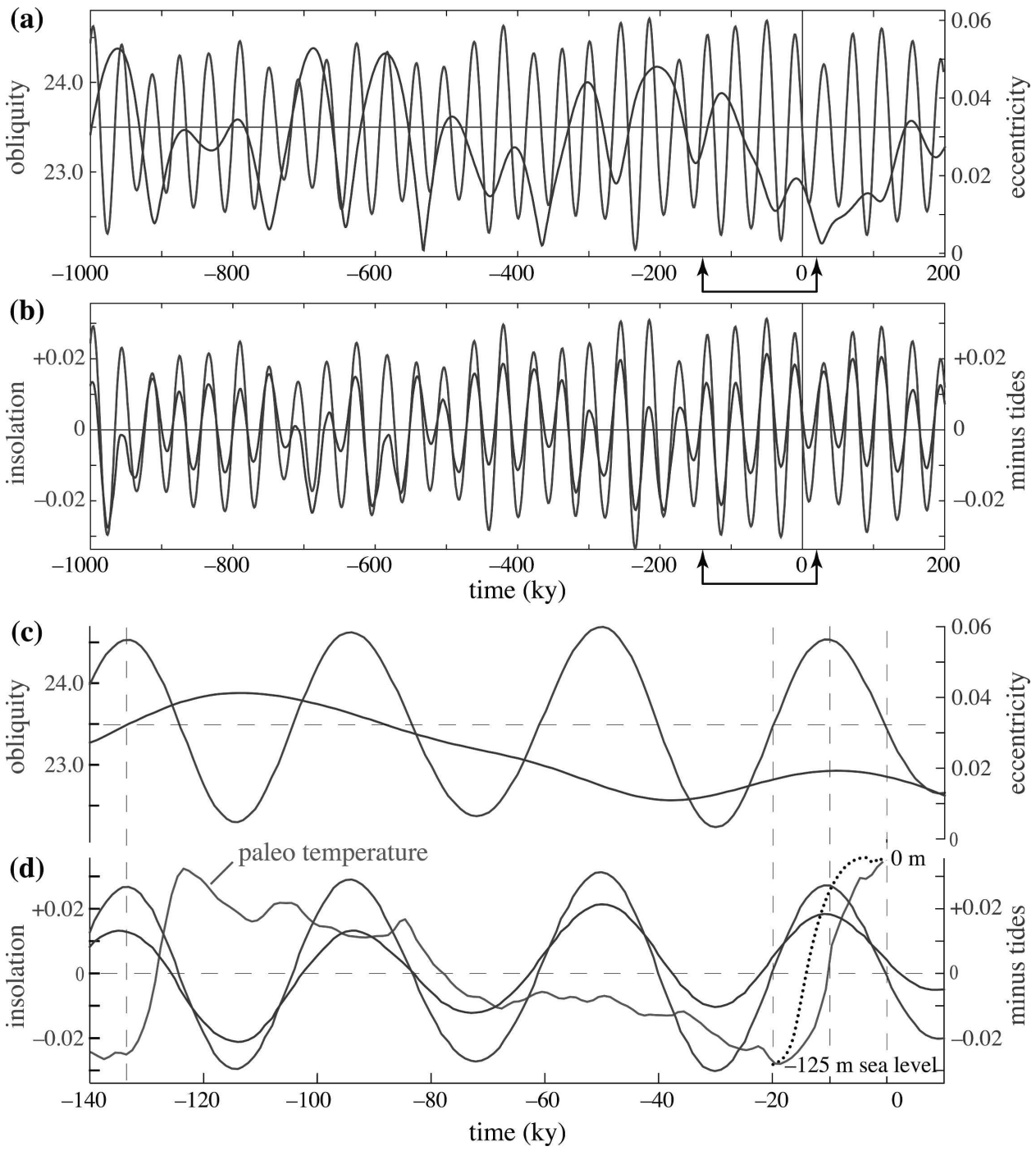

FIG. 5. Obliquity and eccentricity on (a) 1×10^6 yr and (c) 140 000-yr time scales. Associated fractional departures in the average polar insolation and semidiurnal tidal energy [drawn positive downward for ready comparison in (c) and (d)]. The departures are relative to a mean obliquity of $\varepsilon = 23.50$ and eccentricity $\varepsilon = 0.006$ (present values are 23.5 and 0.018). In a linear world with meridional heat flux proportional to equilibrium tidal energy, the curves would be additive. Curves in (d) also show paleotemperature (green) and sea level (dotted) for the last two "terminations." Maximum obliquity and minimum equilibrium tidal energy occur well after the start of termination at −20 kyr.

melt enough ice to raise the sea level by 120 m. This corresponds to only 300 yr of the 10^{15} W flux. A 3% increase in the MOC heat flux could account for the entire melting.

Acknowledgments. We are grateful to the reviewer (Peter Huybers) for his critical review and for many positive recommendations. We thank Chris Garrett, Rob Pinkel, and Harper Simmons for having put us straight on many issues; so has Carl Wunsch, unaware that he was to be the victim of this missile.

One of us (WM) was the recipient of a 65th birthday celebration on 19 October 1982, organized by Chris and Carl. On that morning, I telephoned Carl at the Massachusetts Institute of Technology (MIT) for advice on some manuscript, unaware that he had spent the night in our basement guest room. Carl's secretary professed ignorance of his whereabouts, and when I called Marjory she said, "Carl does not always tell me where he is going."

Carl's contribution to the birthday volume was *Acoustic Tomography and Other Answers* (Wunsch 1984). The "other answers" in this title refer to "9-W" and two other answers from which one was to infer the question by "inverse theory" (IT). Carl had recently embarked on his lifelong obsession with IT. If you cannot infer the question corresponding to "9-W," you can blame it on a defect of IT.

The other part of the title, acoustic tomography, refers to our joint efforts to rely on the intrinsic properties of ocean acoustics for monitoring ocean variability, and was to result in eight joint papers and a book. At one time we thought that the combined application of satellite altimetry (Carl's major contribution to ocean observation) and acoustic tomography would become the cornerstones for large-scale ocean monitoring, but this has not been the case, not yet.

We have shared so many interests since Carl, then a Stommel graduate student, first showed up at my doorstep in 1966 to have a look at tides. We both have had three sabbaticals at the University of Cambridge, the last jointly in 1981–82, and 40 years of friendship. Walter Munk holds the Secretary of the Navy Chair in Oceanography.

REFERENCES

Alford, M. H., and R. Pinkel, 2000: Observations of overturning in the thermocline: The context of ocean mixing. *J. Phys. Oceanogr.,* **30,** 805–832.

Bell, T. H., 1975: Lee waves in stratified flows with simple harmonic time dependence. *J. Fluid Mech.,* **67,** 705–722.

Cartwright, D. E., and R. J. Taylor, 1971: New computations of the tide-generating potential. *Geophys. J. Roy. Astron. Soc.,* **23,** 45–74.

Cox, C., and H. Sandstrom, 1962: Coupling of surface and internal waves in water of variable depth. *J. Oceanogr. Soc. Japan,* **20,** 499–513.

Croll, J., 1890: *Climate and Time in their Geological Relation: A Theory of Secular Changes of the Earth's Climate.* 2d ed. Appleton, 577 pp.

Darwin, G. H., 1911: *The Tides and Kindred Phenomena in the Solar System.* 3d ed. Murray. (Republished in 1962 by W. H. Freeman, 378 pp.)

Doodson, A. T., 1921: The harmonic development of the tide-generating potential. *Philos. Trans. Roy. Soc. London,* **A100,** 305–329.

Egbert, G. D., and R. D. Ray, 2001: Estimates of M_2 tidal energy dissipation from TOPEX/POSEIDON altimeter data. *J. Geophys. Res.,* **106,** 22 475–22 502.

——, ——, and B. G. Bills, 2004: Numerical modeling of the global semidiurnal tide in the present day and in the last glacial maximum. *J. Geophys. Res.,* **109,** CO3003, doi:10.1029/2003JC001973.

Ffield, A. L., and A. Gordon, 1996: Tidal mixing signatures in the Indonesian Seas. *J. Phys. Oceanogr.,* **26,** 1924–1937.

Garrett, C., 1979: Mixing in the ocean interior. *Dyn. Atmos. Oceans,* **3,** 239–265.

——, 2003: Internal tides and ocean mixing. *Science,* **301,** 1858–1859.

Godin, G., 1972: *The Analysis of Tides.* University of Toronto Press, 264 pp.

Hays, J. D., J. Imbrie, and N. J. Shackleton, 1976: Variations in the earth's orbit: Pacemaker of the ice ages. *Science,* **194,** 1121–1132.

Huybers, J., and C. Wunsch, 2005: Obliquity pacing of the late Pleistocene glacial terminations. *Nature,* **434,** 491–494.

Ledwell, J. R., E. T. Montgomery, K. L. Polzin, L. C. St. Laurent, R. W. Schmitt, and J. M. Toole, 2000: Evidence for enhanced mixing over rough topography in the abyssal ocean. *Nature,* **403,** 179–182.

Loder, J. W., and C. Garrett, 1978: The 18.6-year cycle of sea surface temperature in shallow seas due to variations in tidal mixing. *J. Geophys. Res.,* **83,** 1967–1970.

Merrifield, M. A., D. E. Holloway, and T. M. S. Johnston, 2001: The generation of internal tides at the Hawaiian Ridge. *Geophys. Res. Lett.,* **28,** 559–562.

Milanković, M., 1941: *Kanon der Erdbestrahlung und Seine Anwendung auf das Eiszeitenproblem (Canon of Insolation of the Earth and Its Application to the Ice-Age Problem).* Royal Serbian Academy, 484 pp.

Munk, W., 2002: Twentieth century sea level: An enigma. *Proc. Natl. Acad. Sci. USA,* **99,** 6550–6555.

——, and D. E. Cartwright, 1966: Tidal spectroscopy and prediction. *Philos. Trans. Roy. Soc. London,* **A259,** 533–581.

——, and C. Wunsch, 1998: Abyssal recipes II: Energetics of tidal and wind mixing. *Deep-Sea Res. I,* **45,** 1977–2010.

Pettersson, O., 1930: The tidal force. *Geogr. Ann.,* **12,** 261–322.

Pinkel, R., and Coauthors, 2000: Ocean mixing studied near the Hawaiian Ridge. *Eos, Trans. Amer. Geophys. Union,* **81,** 545–553.

Polzin, K. L., J. M. Toole, and R. W. Schmitt, 1995: Finescale parameterization of turbulent dissipation. *J. Phys. Oceanogr.,* **25,** 306–328.

——, ——, J. R. Ledwell, and R. W. Schmitt, 1997: Spatial vari-

ability of turbulent mixing in the abyssal ocean. *Science,* **276,** 93–96.

Rubincam, D. P., 1994: Insolation in terms of the earth's orbital parameters. *Theor. Appl. Climatol.,* **48,** 195–202.

Simmons, H. L., R. W. Hallberg, and B. K. Arbic, 2004a: Internal wave generation in a global baroclinic tide model. *Deep-Sea Res. II,* **51,** 3043–3068.

——, S. R. Jayne, L. C. St. Laurent, and A. J. Weaver, 2004b: Tidally driven mixing in a numerical model of the ocean general circulation. *Ocean Modell.,* **6,** 245–263.

St. Laurent, L. C., and C. Garrett, 2002: The role of internal tides in mixing the deep ocean. *J. Phys. Oceanogr.,* **32,** 2882–2899.

Wunsch, C., 1984: Acoustic tomography and other answers. *A Celebration in Geophysics and Oceanography—1982, in Honor of Walter Munk,* SIO Reference Series 84-05, Scripps Institution of Oceanography, 47–62.

——, 2000: On sharp spectral lines in the climate record and the millennial peak. *Paleoceanography,* **15,** 417–424.

——, 2002: The spectral description of climate change including the 100KY energy. *Climate Dyn.,* **20,** 353–363.